ENVIRONMENTAL RESEARCH
LETTERS

PURPOSE-LED PUBLISHING™

Celebrating the 20th anniversary of Environmental Research Letters

LETTER • OPEN ACCESS

Asymmetric ENSO teleconnections in a symmetric CO_2 concentration pathway

To cite this article: Soon-Il An *et al* 2024 *Environ. Res. Lett.* **19** 124028

View the article online for updates and enhancements.

You may also like

- Projected ENSO teleconnection on the Southeast Asian climate under global warming
Dzung Nguyen–Le
- The El Niño–Southern Oscillation teleconnection to southern Africa in a changing climate
Jessica Steinkopf and Francois Engelbrecht
- Vulnerability of sorghum production to extreme, sub-seasonal weather under climate change
M Eggen, M Ozdogan, B Zaitchik et al.

SmarAct | group

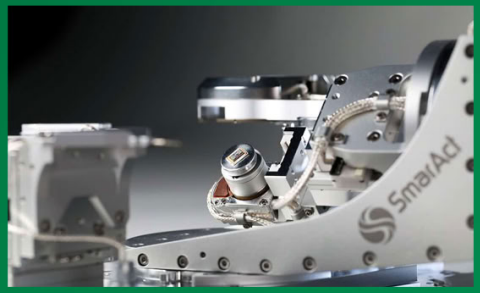
webinar

More details and registration

One sample, many dimensions: prospects for multimodal nanoscale characterization

Explore how precise sample manipulation enables complementary nanoscale techniques to work together on one sample

Live at 2 p.m. GMT/3 p.m. CET,
12 November 2026



This content was downloaded from IP address 58.23.54.233 on 13/11/2026 at 12:33

IOP Publishing Environ. Res. Lett. 19 (2024) 124028 https://doi.org/10.1088/1748-9326/ad7b5c

ENVIRONMENTAL RESEARCH
LETTERS

LETTER

Asymmetric ENSO teleconnections in a symmetric CO_2 concentration pathway

Soon-Il An[1,2,3,*], **Su-Hyeon Shin**[2], **Chao Liu**[1], **Sang-Wook Yeh**[4], **Seung-Ki Min**[3], **Seok-Woo Son**[5], **Jong-Seong Kug**[5] and **Jae-Heung Park**[5]

[1] Irreversible Climate Change Research Center, Yonsei University, Seodaemun-gu, Seoul 03722, Republic of Korea
[2] Department of Atmospheric Sciences, Yonsei University, Seodaemun-gu, Seoul 03722, Republic of Korea
[3] Division of Environmental Science and Engineering, Pohang University of Science and Technology (POSTECH), Pohang, Republic of Korea
[4] Department of Marine Sciences and Convergence Engineering, Hanyang University ERICA, Ansan, Republic of Korea
[5] School of Earth and Environmental Sciences, Seoul National University, Seoul, Republic of Korea
[*] Author to whom any correspondence should be addressed.

E-mail: sian@yonsei.ac.kr

Keywords: hysteresis of ENSO teleconnections, CO_2 removal scenario, ITCZ

Supplementary material for this article is available online

OPEN ACCESS

RECEIVED
10 June 2024

REVISED
27 August 2024

ACCEPTED FOR PUBLICATION
16 September 2024

PUBLISHED
5 November 2024

Original content from this work may be used under the terms of the Creative Commons Attribution 4.0 licence.

Any further distribution of this work must maintain attribution to the author(s) and the title of the work, journal citation and DOI.

Abstract

El Niño-Southern Oscillation (ENSO) is the strongest interannual phenomenon occurring in the tropical Pacific, significantly affecting the entire world. The ENSO response to increasing CO_2 concentrations have been extensively studied, but the reverse scenario is still not well understood. Here, we investigate the hysteresis of ENSO teleconnections in a CO_2 removal simulation of an earth system model. During the ramp-up period of CO_2 concentrations, Pacific-North American and Pacific-South American patterns are intensified, with the eastward shift of their poles, which are even further intensified during the ramp-down period. This ENSO teleconnection hysteresis is closely linked to the tropical-origin hysteresis, in which, during the ramp-down periods, the prevalence of the eastern-Pacific type El Niño leads to the hysteresis in the eastern Hemispheric ENSO teleconnections and the enhanced ENSO skewness and the eastward shift of ENSO-induced tropical atmospheric convection do to that in the western Hemispheric ENSO teleconnection. The alterations by the tropical origin are predominantly associated with intensified southward migration of the Intertropical Convergence Zone, along with a stronger El Niño-like warming trend. We also demonstrate that the hysteretic change in the mid-latitude mean state over the North Pacific region could lead to hysteresis of the ENSO teleconnection without invoking a tropical origin.

1. Introduction

El Niño-Southern Oscillation (ENSO) is the strongest interannual climate phenomenon that occurs in the tropical Pacific Ocean, and it has a marked impact on socioeconomic conditions globally through its atmospheric and oceanic teleconnections (Yeh *et al* 2014, Timmermann *et al* 2018). Due to the critical need to understand the impacts of climate change and explore adaptation strategies, numerous studies have been conducted on the future ENSO projections (Collins *et al* 2010, Kim *et al* 2014, Cai *et al* 2022, Olson *et al* 2022). However, the confidence level regarding the projected changes in ENSO variability for the 21st century remains at a medium level (Kim *et al* 2014, Arias *et al* 2021). There are large uncertainties in projecting its future behavior using climate models, due to internal variability, biases in the mean state, and insufficient understanding and modeling of ENSO physics (Beobide-Arsuaga *et al* 2021, Hyun *et al* 2022). For instance, most state-of-the-art climate models have predicted an El Niño-like warming trend (Yan *et al* 2020), whereas the observed tropical Pacific sea surface temperature (SST) indicates

© 2024 The Author(s). Published by IOP Publishing Ltd

the La Niña-like warming trend (Kohyama *et al* 2017). Nevertheless, the Intergovernmental Panel on Climate Change 6th Assessment Report (IPCC AR6; Arias *et al* 2021) highlighted that rainfall variability related to ENSO will very likely increase. This enhanced rainfall variability is expected to lead to significant regional climate change through changes in ENSO teleconnection. This underscores the complexities in predicting ENSO's future impacts, as well as the significant role it plays in influencing global climate patterns.

Under a global warming condition, ENSO-driven tropical precipitation anomalies are projected to shift and extend eastward (Yan *et al* 2020), possibly due to warming of the background SST and associated changes in the atmospheric circulations (Kug *et al* 2010, Cai *et al* 2014, Power *et al* 2014) as well as changes in circulation anomalies induced by ENSO itself (Hoskins and Karoly 1981, Huang and Xie 2015). The eastward shift of ENSO-induced precipitation anomalies is expected to modify the atmospheric teleconnection patterns over both the Northern and Southern Hemispheres (Perry *et al* 2017, Yeh *et al* 2018), as these changes influence the pathway of Rossby waves (Hoskins and Karoly 1981). Specifically, the major ENSO teleconnection patterns, such as Pacific-North American (PNA) and Pacific-South American (PSA), are anticipated to shift eastward and intensify in response to the eastward migration of ENSO-induced tropical precipitation anomalies under global warming (Cai *et al* 2021, Wang *et al* 2022). Apart from the changes in the tropical climate anomalies, the background mid-latitude circulation is also decisive in the positioning of the ENSO teleconnection pattern (Ting and Yu 1998, Wang *et al* 2021), influencing mid-latitude synoptic systems along the mid-latitude waveguides (O'Kane *et al* 2017).

Recently, based on the Community Earth System Model version 1.2 (CESM1.2) large-ensemble simulation adopting CO_2 ramp-up and ramp-down scenario (CDR-reversibility experiment), Liu *et al* (2023a, 2023b) showed that ENSO amplitude and skewness and its global teleconnection patterns exhibit strong hysteretic behaviors. Both PNA and PSA patterns further strengthen and shift eastward during the ramp-down period compared to the ramp-up period, which results in the hysteresis in ENSO teleconnections. Neverthless, as of now, research on hysteresis in ENSO teleconnections is notably scarce. Furthermore, the governing mechanisms behind this phenomenon remain unexplored. Using the CDR-reversibility experiment, we investigate the hysteresis of ENSO teleconnections to shed light on its underlying mechanism.

2. Methods

2.1. CESM1.2 experiment

The CESM1.2 (Hurrell *et al* 2013) consists of the atmosphere (Community Atmospheric Model version 5), ocean (Parallel Ocean Program version 2), sea ice (Community Ice Code version 4), and land models (Community Land Model version 4). The atmosphere and ocean models have a horizontal resolution of approximately $1\ \times 1^\circ$ and 30 vertical levels (Neale *et al* 2012), and $1\ \times 0.5^\circ$ with 60 vertical levels (Smith *et al* 2010), respectively. The land model incorporates the carbon-nitrogen cycle (Lawrence *et al* 2011).

We employed two idealized CO_2 pathways. The first (PD experiment) involves maintaining a constant CO_2 concentration level of 367 ppm, spanning 900 years, with a present-day climate simulation. The second (CDR-reversibility experiment; An *et al* 2021), consisting of 28 ensemble members, involves a 1% annual increase in CO_2 concentration for 140 years until quadrupling (i.e. 1468 ppm; ramp-up period; RU), then a symmetric decrease pathway for 140 years until returning to its initial state (ramp-down period; RD). Afterwards, a constant CO_2 simulation is conducted for 220 years (restoring period). Here, the model's capability to simulate ENSO teleconnections is validated by comparing the observational data with the PD experiment, where a strong similarity is observed (supplementary figure S1).

The asymmetrical response of ENSO teleconnections to symmetric forcing indicates that trends in ENSO teleconnection during RD are not simply mirror images of those during RU. Therefore, the asymmetric change in ENSO teleconnections can be referred to as the hysteresis of ENSO teleconnections.

Here, the ENSO teleconnections were identified as the regression of 500 hPa geopotential height (GPH) anomalies against Niño-3.4 index (SST anomalies averaged over 5 °N–5 °S, 170 °–120 °W) using each ensemble of the CDR-reversibility experiment, and then took an average of them. Therefore, the modulation of ENSO teleconnections by natural variability was removed. The Outgoing Longwave Radiation (OLR) was used as a proxy for the convective activity. Changes in the zonal locations and intensity of ENSO are quantified by ENSO indices, including Niño-3 (5 °N–5 °S, 150 °–90 °W), Niño-3.4 (5 °N–5 °S, 170 °–120 °W), and Niño-4 (5 °N–5 °S, 160E °–150 °W). All analysis in this study rely exclusively on mean values for the boreal winter (December, January, and February).

2.2. Linear baroclinic model (LBM) experiment

The role of mid-latitude mean state change on ENSO teleconnections is investigated using a linear

baroclinic model. The LBM is a global, time-dependent primitive equation model linearized at a specific state, with a horizontal resolution of T42 and 20 sigma levels (Watanabe and Kimoto 2000). Here, the model is integrated for 50 d, with the analysis based on the average for the last 30 d.

To identify ENSO teleconnections, two experiments were conducted to apply idealized forcings for El Niño and La Niña. The core of atmospheric diabatic heating was determined based on 500 hPa divergence. The idealized heating was applied in an elliptical shape, with a major axis of 30 degrees in longitude and a minor axis of 15 degrees in latitude at the 0.6 sigma level. The results from the LBM experiments for El Niño and La Niña were then combined to identify the ENSO teleconnection, representing the sum of the El Niño and La Niña teleconnections.

3. Results

3.1. Asymmetric ENSO teleconnections in the symmetrical CO_2 pathway

First, the teleconnection features for a period of 30 years at the center of the year of doubling CO_2 concentration ($2XCO_2$) levels of the RU and RD are compared (figure 1). Figures 1(a) and (b) reveal that the ENSO teleconnections are characterized by a wave-train pattern, resembling the PNA pattern. However, during RU, the poles of PNA pattern are not only deepened but also slightly shifted eastward compared to the PD experiment. In RD, these poles move even farther eastward (see supplementary figure S2(a)). Consequently, an increase in 500 hPa GPH anomalies over the north Pacific and a decrease over the North American continent are observed, highlighting as the asymmetric ENSO teleconnection at the same CO_2 level but under different CO_2 pathways (figure 1(c)).

Similar features are observed in the Southern Hemisphere, particularly the eastward shift of PSA patterns (figures 1(d) and (e)). The conventional PAS pattern is represented by an eastward-propagating wave train extending from eastern Australia to Argentina (Lou *et al* 2021). The asymmetry in ENSO teleconnections in the Southern Hemisphere is identified as the farther eastward shift of wave trains (supplementary figure S2(b)), dominated by a wave number 2 pattern (figure 1(f)). This asymmetric ENSO teleconnections in response to symmetrically changing climate forcing clearly indicate the presence of hysteresis in ENSO teleconnections.

To obtain the hysteresis map of ENSO teleconnections, a 30 year moving regression of 500 hPa GPH anomalies against the Niño-3.4 index was computed for each ensemble of the CDR-reversibility experiment, and then the ensemble mean was taken. From a 30 year moving regression, the linear trend of ENSO teleconnections is separately calculated for RU and RD. By adding these two trends (center panel of figure 2), their symmetric parts are cancelling out, the residual serves as a metric for the intensity of asymmetric ENSO teleconnections to a symmetric CO_2 pathway. The area-averaged teleconnection (30 year moving regression) values for the selected dominant regions of ENSO teleconnection hysteresis are represented in figure 2. In all boxes, the ensemble spread for RD exhibits sparse overlap with that for RU, especially in a low CO_2 concentration regime (see also supplementary figure S3). Yet, the behaviors of each box are quite different to each other. As in figure 1, a strong hysteresis of the ENSO teleconnections is observed in the North Pacific (box 1) and North America (box 2) in the Northern Hemisphere while the hysteresis response of the Southern Hemisphere is characterized by a wave number two pattern (boxes 3–6). Note that a positive (negative) value represents an enhanced positive (negative) trend of the ENSO teleconnection during RD compared to RU.

3.2. Mechanism of ENSO teleconnection hysteresis

The changes in the ENSO-induced atmospheric wave sources over the tropical Pacific could change ENSO teleconnections. Therefore, the ENSO-related tropical SST and convection changes could be a major factor in driving the ENSO teleconnection hysteresis. First, the intensity, type, asymmetry, atmospheric convection anomalies, and the center of the maximum atmospheric convection of ENSO are quantified as the standard deviations (STD) of Niño-3.4 index, Niño-3 STD minus Niño-4 STD ($N3^2$–$N4^2$), and Niño-3.4 skewness, the minimum regression value of OLR against Niño-3.4 index, and its longitudinal location along the equatorial band of 5°S–5°N, respectively. Then, changes of these values are compared with the hysteresis of ENSO teleconnections. Before assessing, the 30 year moving averages were taken for each variable to match the timescale with ENSO teleconnection computation.

Both Niño-3.4 STD and the OLR minimum increase as CO_2 increases (figures 3(a), and (d)). However, near at $4XCO_2$ level (year 2140), Niño-3.4 STD starts to decrease and later the OLR minimum also decreases. During the RD, the Niño-3.4 STD shows signs of recovery, while the OLR minimum remains with almost no change. Such different behaviors of these two variables might be associated with the enhancement of El Niño-like warming, which is more pronounced during RD (figure 4(a); Liu *et al* 2023b). Consequently, the elevated background SST could sustain stronger atmospheric convection even with small Niño-3.4 STD.

The $N3^2$–$N4^2$ identifies a dominant ENSO-type between the central Pacific and eastern Pacific ENSOs (Shin *et al* 2022). It exhibits a minimal change during RU, and then quickly increases during the early RD and remains afterward (figure 3(b)). Hence, during the RU, while the zonal location of the maximum

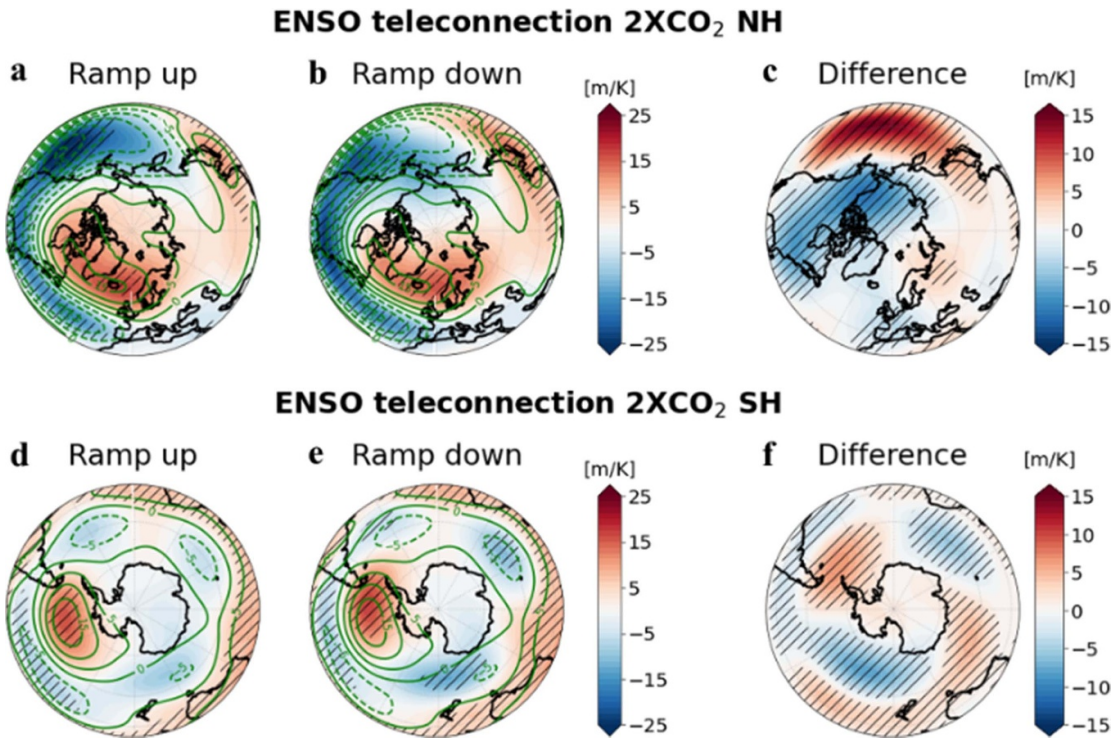


Figure 1. Regression of 500 hPa geopotential height (GPH) anomalies against Niño-3.4 index (SST anomalies averaged over 5 °S–5 °N, 170 °–120 °W) obtained from each ensemble of CESM1.2 Present-day, ramp-up and ramp-down experiments, and then took an average of them. (a) and (b) over Northern Hemisphere for 30 year period at the center of $2XCO_2$ level in ramp-up and ramp-down, respectively. (d) and (e) Same as (a) and (b), respectively, but for Southern Hemisphere. (c) and (d) are difference between the ramp-down and ramp-up (Ramp-down minus Ramp-up). Contours in (a), (b), (d) and (e) represent the regression for Present-day simulation with 5 meter interval. Units are mK^{-1}. Hatched areas for (a), (b), (d) and (e) indicate statistically significant at 95% confidence based on the two tailed Wald test with t-distribution where more than 25 ensembles are significant at 95% confidence. Hatched areas for (c) and (f) indicate statistically significant at 95% confidence based on the two tailed student's t-test.

SST variability undergoes slight changes, the El Niño-like warming trend (figure 4(a)) promotes the eastward shift of the OLR centroid from the dateline to 160 °W. Due to the continuous strengthening of El Niño-like warming in the early RD, the OLR centroid moves farther eastward. Afterward, despite the weakening of El Niño-like warming, the increased Niño-3 variability (large $N3^2$–$N4^2$) maintains the portion of the OLR centroid to stay around 160 °W (figure 3(e)).

Finally, the hysteresis of Niño-3.4 skewness is also distinct such that Niño-3.4 skewness keeps decreasing until the middle of the RD, and then slightly increases from negative to zero (figure 3(c)), closely resembling the meridional movement of ITCZ (Liu *et al* 2023b). The teleconnections associated with El Niño and La Niña exhibit asymmetry in both location and amplitude. This asymmetry is also observed in our simulations (supplementary figure S4). The asymmetric teleconnections could generate the long-term climate variability through nonlinear rectification (An *et al* 2007). Therefore, the hysteresis in Niño-3.4 skewness could be a cause for the hysteresis in ENSO teleconnections.

The relationship in hysteresis between ENSO characteristics and teleconnections is measured as a correlation between changes in ENSO characteristics (all elements outlined in figure 3) and corresponding changes in ENSO teleconnections over each box in figure 2. As shown in table 1, the time series of each box are significantly correlated to one or two indices. Box 1 (North Pacific) is significantly positively correlated to the $N3^2$–$N4^2$, and thus their temporal evolutions are remarkably similar (compare figures 2 and 3(b)). As the ENSO variability is more confined over Niño-3 region, i.e. increasing $N3^2$–$N4^2$, during RD, the deepening of the low center over the western North Pacific by El Niño becomes weaker. While the opposite pattern by La Niña remains. Therefore, the positive tendency of ENSO teleconnection over western North Pacific (box 1) is enhanced through CO_2 pathway.

For box 2 (North America), the largest correlation is observed with the OLR centroid with 95% confidence, and secondly both the $N3^2$–$N4^2$ and Niño-3.4 skewness are correlated with 90% confidence. Therefore, the hysteresis in ENSO teleconnection over North America is primarily related to the zonal displacement of the atmospheric convection center, with additional contributions of the ENSO-type change and El Niño-La Niña asymmetry. Note that, during RD, the Niño-3.4 skewness is reduced and even

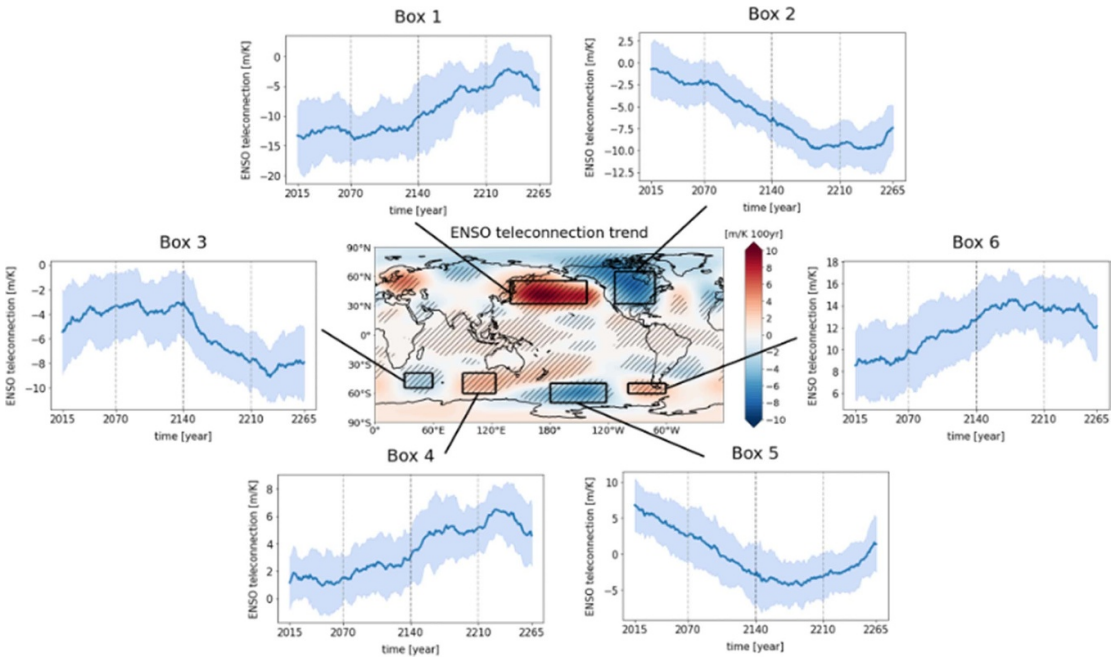


Figure 2. Sum of ENSO teleconnection trends of 500 hPa GPH anomalies for both ramp-up and ramp-down periods (center), referring the ENSO teleconnection hysteresis map. ENSO teleconnection trends were calculated by using the 30 year moving regressions of 500 hPa GPH anomalies at each grid point against Niño-3.4 index for ramp-up and ramp-down of CDR-reversibility experiment, separately, and then the asymmetry of ENSO teleconnection trends is identified by adding ENSO teleconnection trend for the ramp-up and that for the ramp-down. The hatched areas indicate statistical significance at 95% confidence based on the two-tailed student t-test. All calculations have been done by using 28 ensembles independently and then the ensemble mean was computed (solid line in each panel). Boxes in the central map indicate the area to be averaged, and the time series of the areal-mean regression values for each box are shown in the surrounded panels. Cross-dashed lines indicate 2070, 2140, and 2210 model years, which are the timings for $2XCO_2$ in ramp-up period, $4XCO_2$, and $2XCO_2$ in ramp-down period. Units are $mK^{-1}100\ yr^{-1}$. Color shadings indicate the ensemble spread of one standard deviation.

becomes negative, indicating that the impact of La Niña is relatively enhanced (figure 3(c)).

In the Southern Hemisphere, box 3 is correlated to $N3^2$–$N4^2$ (95% confidence), whereas box 4 does to both $N3^2$–$N4^2$ (95% confidence) and OLR centroid (90% confidence). These two boxes are located over the Southern Indian Ocean. ENSO teleconnection over southern Indian Ocean is very weak during RU, but it becomes stronger during RD (figure 1(f)). Therefore, it may be related to the relatively enhanced Niño-3 SST variability. While boxes 5 and 6 over the South Pacific Ocean, collocating with PSA pattern, are correlated to OLR centroid and ENSO skewness with an opposite sign (95% confidence). Therefore, the systematic shift of ENSO-induced atmospheric convection leads to a similar shift of PSA, which results in the hysteresis of these ENSO teleconnections. The horizontal pattern of Niño-3.4 skewness is dominated by the east-west contrast pattern over the tropical Pacific (Liu *et al* 2023b), and thus the enhanced (suppressed) positive skewness corresponds to an eastward (westward) shift of anomalous atmospheric convection. Since ENSO skewness is strongly reduced during RD (figure 3(c)), the westward migration of ENSO-induced atmospheric convection is expected. However, ENSO-induced atmospheric convection moved to the east (e.g. figure S5) because the reduction of ENSO skewness mainly results from the enhanced ENSO variability (Liu *et al* 2023b).

For additional validation, we calculated the correlations with the same variables but for each ensemble, and averaged them (table 1). Generally, the average of the ensemble-based correlations aligns with the correlation derived from the ensemble-mean. Yet, due to the substantial ensemble spread, the former is overall smaller than the latter. A notable exception arises in Niño-3.4 skewness, where the correlation based on the ensemble mean is significant, but the ensemble-based correlation is minimal. The Niño-3.4 skewness, being a result of ENSO's nonlinearity, is relatively less influenced by external forcings. Therefore, the ensemble spread appears to be very large (supplementary information table S2), leading to a reduction in the ensemble average.

3.3. Tropical mean state change and its impact on ENSO characteristics

Here, we investigate how the mean state over the tropical Pacific alters ENSO characteristics. As CO_2 concentrations increase, the tropical Pacific SST increases over the whole basin and thus, the warm pool expands to the east (figure 4(a)). The maximum warming is observed during the early RD, and the tropical Pacific during RD is warmer than that during RU. The warm

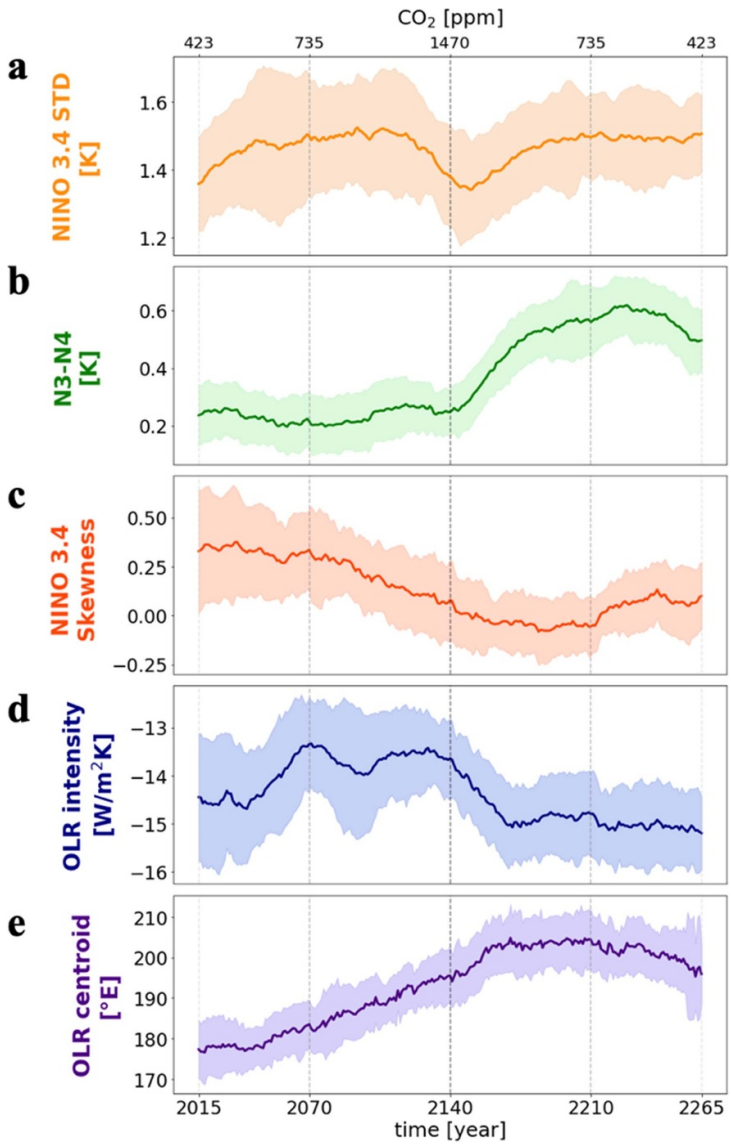


Figure 3. Timeseries of 30 year moving (a) standard deviation (STD) of Niño-3.4 (K); (b) Niño-3 STD minus Niño-4 STD (K); (c) Niño-3.4 skewness (non-dimensional unit); (d) Minimum regression values of outgoing longwave radiation (OLR) against Niño-3.4 index ($Wm^{-2}\,K^{-1}$); and (e) As in (d) but for its longitudinal centroid (longitudinal degree), obtained from CDR-reversibility simulations of CESM1.2. All quantities are DJF-mean. Shadings indicate the ensemble spread of one standard deviation.

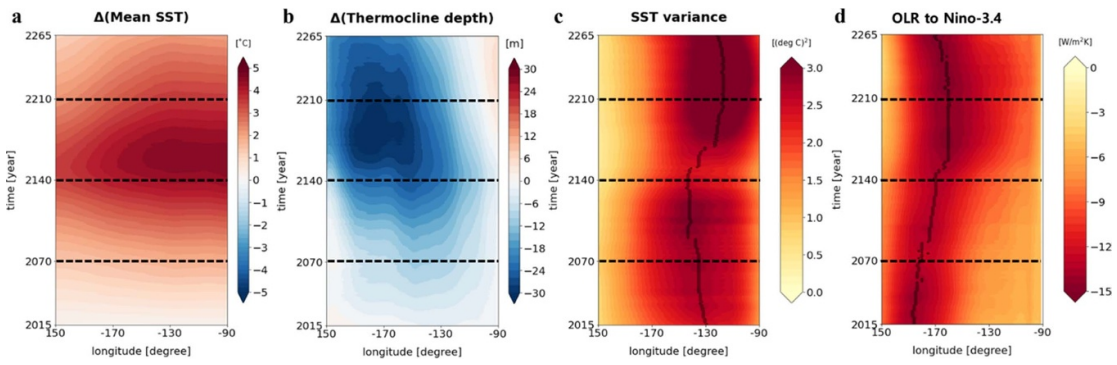


Figure 4. (a) Time-longitude section plot of deviation of 30 year moving mean SST (shading) from PD mean (°C). (b) As in (a) expect for mean thermocline depth. (c) Time-longitude section plot of SSTA variance (shading; $°C^2$). (d) As in (c) except for OLR regression to Niño-3.4 (contour; $Wm^{-2}K^{-1}$) along the equator (5 °S–5 °N). The thick line in (c) indicates the longitude for the corresponding maximum value, and that in (d) indicates its minimum value.

Table 1. Correlation coefficients between various tropical Pacific physical quantities (uppermost row) and ENSO teleconnection trends over boxes (leftmost column) based on ensemble-mean values. Over 90% and 95% confidence correlation based on the minimum degree of freedom (degree of freedom = 2) are indicated by * and **, respectively. Numbers in parenthesis indicate ensemble average of correlation coefficients of each ensemble between various tropical Pacific quantities and ENSO teleconnection trends over boxes.

	Niño-3.4 STD (ENSO intensity)	Niño-3 STD minus Niño-4 STD (Type of ENSO)	Niño-3.4 skewness (ENSO asymmetry)	ENSO-induced OLR Minimum (Convection Intensity)	OLR centroid (location of atmospheric convection)
Box 1	0.18 (0.06)	0.97** (0.63)	−0.73 (−0.22)	−0.84 (−0.26)	0.84 (0.54)
Box 2	−0.08 (−0.02)	−0.90* (−0.68)	0.93* (0.41)	0.64 (0.28)	−0.98** (−0.73)
Box 3	−0.22 (−0.1)	−0.97** (−0.55)	0.61 (0.22)	0.89 (0.24)	−0.73 (−0.43)
Box 4	0.07 (−0.03)	0.95** (0.6)	−0.82 (−0.25)	−0.76 (−0.29)	0.92* (0.57)
Box 5	0.08 (−0.05)	−0.63 (−0.53)	0.95** (0.27)	0.29 (0.02)	−0.94* (−0.65)
Box 6	−0.04 (0.05)	0.79 (0.53)	−0.96**(−0.23)	−0.52 (−0.13)	0.98** (0.53)

pool expansion indicates an expansion of the convectively unstable region. Therefore, the anomalous atmospheric convection center (figure 4(d)) and SST anomalies (figure 4(c)) are shifted to the east.

The eastward shift of the ENSO action center results in a longer ENSO period due to the slower oceanic adjustment (An and Wang 2000) and the greater thermocline feedback over the eastern Pacific (An and Jin 2000, An *et al* 2012), leading to increased ENSO variability. Nevertheless, there is a tendency for the oscillation period of Niño-3.4 to decrease, during RD (An *et al* 2022), suggesting that the first case may not be applicable. In terms of thermocline feedback, the reduced zonal SST gradient over the tropical Pacific leads to a weaker trade wind, which can deepen the mean thermocline over the tropical eastern Pacific (figure 4(b)) and enhance the ENSO amplitude (An and Jin 2001, An *et al* 2008). Moreover, the eastward-expanded zonal wind anomaly linked with the eastward shift of anomalous atmospheric convection drives a stronger response to the thermocline anomaly, consequently intensifying ENSO. Concerning ENSO skewness, Liu *et al* (2023b) claimed that the southward migration of ITCZ in CO_2 pathway (Kug *et al* 2022) during RD might reduce the skewness of SST anomaly in the central and eastern Pacific.

Generally, during El Niño (La Niña), the precipitation and OLR anomalies in the central-eastern Pacific tend to move eastward (westward). In our simulations, El Niño change shows a significant hysteresis, but La Niña does not. Therefore, the hysteresis of zonal displacement of precipitation (OLR as well) anomalies rely mainly on hysteresis of El Niño. The El Niño-related precipitation anomalies in the central-eastern Pacific continuously intensify and move eastward until the middle of the RD (figure S5), and thus further favoring positive SST anomaly increases.

3.4. Mid-latitude mean state change and its impact on ENSO teleconnections

Here, we consider a possible modification of ENSO teleconnection by changes in the mid-latitude mean atmospheric circulation. Interestingly, the mid-latitude mean atmospheric circulation shows the hysteretic change between RU and RD. Specifically, the north Pacific jet stream at 200 hPa during RD moved to the north in western North Pacific and to the south in the eastern North Pacific, compared to RU (supplementary figure S6(a)). The southward movement of the mid-latitude jet is presumably due to the southward migration of the tropical Pacific ITCZ and the warmer Arctic (Kug *et al* 2022). However, the factors driving the northward movement of the jet remain unclear. Since this point is beyond our scope, we will leave this issue to others. Nevertheless, the barotropic shear instability (Simmons *et al* 1983) caused by the changes in the jet-stream could induce the anomalous anticyclonic circulation over the western North Pacific (supplementary figure S6(b)).

To confirm the hypothesis on the mid-latitude mean state induced modification of ENSO teleconnection, we compute the atmospheric circulation response to the prescribed atmospheric heat sources using LBM, where its background states are prescribed as the 500 hPa wintertime mean winds for $2XCO_2$ period of each RU and RD. The $2XCO_2$ period indicates a period of 30 years centered the year of $2XCO_2$. Two atmospheric wave sources centered at the maximum loading of divergence/convergence in the mid-troposphere for El Niño (115.6 °W, 0.9 °N) and La Niña (117.8 °W, 2.4 °N) were prescribed, and then the responses by two sources were added. As shown in figure 5, even without changing the tropical wave-pumping source, the different mid-latitude backgrounds could generate the asymmetry in ENSO teleconnections between RU and RD with some similarities with CDR-reversibility experiments. Therefore, the hysteretic response of mid-latitude mean states could lead to the hysteresis of ENSO teleconnection without hysteretic change in tropical Pacific. However, due to the limitation of LBM, some discrepancies are also observed.

Although the LBM experiment demonstrated a potential role of the mid-latitude background circulation change in influencing the hysteresis of ENSO teleconnections, several caveats need to be

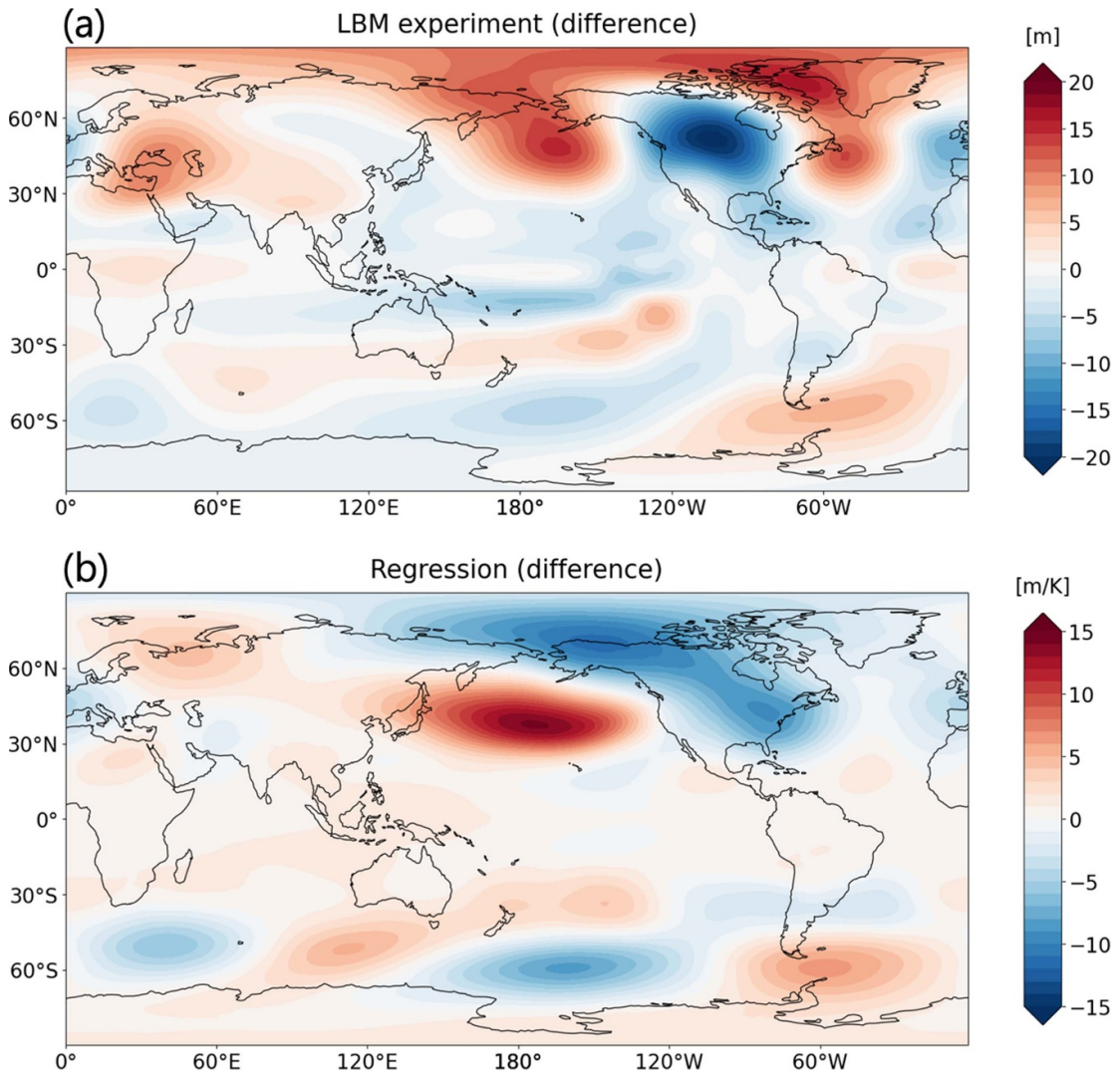


Figure 5. (a) Difference of ENSO teleconnections in 500 hPa geopotential height anomalies combined of both El Niño and La Niña induced effects between the 30 year $2XCO_2$ periods of the ramp-up and those of the ramp-down derived from LBM experiment. (b) As in (a) except for the regression map of 500 hPa geopotential height anomalies with respect to Niño-3.4 index from CESM experiment.

considered. Firstly, the experiment only provides qualitative insights, making it difficult to quantify the effectiveness of mid-latitude effects relative to tropical effects. Secondly, the LBM results over the Northern Hemisphere were rather shifted to the north. Thirdly, the stronger differences in LBM experiments were observed over the north Atlantic, but almost no signals over the same location in CDR-reversibility experiments. To reduce these limitations, more sophisticated methodologies are required, which will be our future project.

4. Summary and discussions

In this study, we analyze the hysteresis in ENSO teleconnections under a CO_2 removal simulation. Major hysteresis of ENSO teleconnections was associated with hysteresis of ENSO characteristics, including the dominant ENSO type, the zonal location of ENSO-induced convection, and ENSO skewness. The hysteresis of ENSO teleconnections over the eastern Hemisphere (boxes 1, 3, and 4 in figure 2) are mainly correlated with the dominant ENSO type, while that over the western Hemisphere (boxes 2, 5, and 6) does with the zonal location of ENSO-induced convection and ENSO skewness. Understanding the distinct hysteresis of ENSO teleconnections between the Eastern and Western Hemispheres is not straightforward. However, a pronounced eastward shift of ENSO variability during RD could initiate significant teleconnections over the western Hemisphere.

Here, we did not demonstrate how changes in the ENSO type could alter the ENSO teleconnection, independently from the changes in the OLR centroid. For atmospheric teleconnections to occur, strong wave pumping by deep convection is required. Therefore, it is difficult to directly explain changes in teleconnections solely based on SST variations. However, the change in ENSO type could induce changes in atmospheric circulation within

the planetary boundary layer without invoking deep convection (Lindzen and Nigam 1987, An 2011), and potentially affect the meridional position of the Pacific ITCZ. The same principle operates on the southward shift of ITCZ during El Niño. Since the meridional movement of ITCZ can change the mid-latitude circulation (Anderson *et al* 2009, Denton *et al* 2010, Ceppi *et al* 2013), it is hypothesized that the ENSO type could influence mid-latitude teleconnections through these processes. Further analysis as a future research is required to thoroughly investigate this hypothesis.

Data availability statement

The data that support the findings of this study are openly available at the following URL/DOI: http://doi.org/10.17632/9ybg2n46yf.1.

Acknowledgment

This work was supported by National Research Foundation of Korea (NRF) grants funded by the Korean government (MSIT) (NRF-2018R1A5A1024958, RS-2023-00208000). S I A was supported by the Yonsei Fellowship, funded by Lee Youn Jae.

Conflict of interest

The authors declare no conflicts of interest relevant to this study

ORCID iDs

Soon-Il An https://orcid.org/0000-0002-0003-429X
Su-Hyeon Shin https://orcid.org/0009-0007-1478-1468
Chao Liu https://orcid.org/0000-0002-3509-5690
Sang-Wook Yeh https://orcid.org/0000-0003-4549-1686
Seung-Ki Min https://orcid.org/0000-0002-6749-010X
Seok-Woo Son https://orcid.org/0000-0003-2982-9501
Jong-Seong Kug https://orcid.org/0000-0003-2251-2579
Jae-Heung Park https://orcid.org/0000-0002-8556-2314

References

An S-I 2011 Atmospheric responses of gill-type and lindzen-nigam models to global warming *J. Clim.* **24** 6165–73
An S-I *et al* 2021 Global cooling hiatus driven by an AMOC overshoot in a carbon dioxide removal scenario *Earth's Future* **9** e2021EF002165
An S-I *et al* 2022 Intensity changes of Indian Ocean dipole mode in a carbon dioxide removal scenario *npj Clim. Atmos. Sci.* **5** 20
An S-I and Jin -F-F 2000 An eigen analysis of the interdecadal changes in the structure and frequency of ENSO mode *Geophys. Res. Lett.* **27** 1573–6
An S-I and Jin -F-F 2001 Collective role of thermocline and zonal advective feedbacks in the ENSO mode *J. Clim.* **14** 3421–32
An S-I, Kim J-W, Im S-H, Kim B-M and Park J-H 2012 Recent and future sea surface temperature trends in tropical pacific warm pool and cold tongue regions *Clim. Dyn.* **39** 1373–83
An S-I, Kug J-S, Ham Y-G and Kang I-S 2008 Successive modulation of ENSO to the future greenhouse warming *J. Clim.* **21** 3–21
An S-I, Kug J-S, Timmermann A, Kang I-S and Timm O 2007 The influences of ENSO on the generation of decadal variability in the North Pacific *J. Clim.* **20** 667–80
An S-I and Wang B 2000 Interdecadal change of the structure of the ENSO mode and its impact on the ENSO frequency *J. Clim.* **13** 2044–55
Anderson R F, Ali S, Bradtmiller L I, Nielsen S H H, Fleisher M Q, Anderson B E and Burckle L H 2009 Wind-driven upwelling in the Southern Ocean and the deglacial rise in atmospheric CO_2 *Science* **323** 1443–8
Arias P A *et al* 2021 *Technical Summary. In Climate Change 2021: The Physical Science Basis. Contribution of Working Group I to the Sixth Assessment Report of the Intergovernmental Panel on Climate Change* ed V Masson-Delmotte *et al* (Cambridge University Press) pp 33–144
Beobide-Arsuaga G *et al* 2021 Uncertainty of ENSO-amplitude projections in CMIP5 and CMIP6 models *Clim. Dyn.* **56** 3875–88
Cai W *et al* 2014 Increasing frequency of extreme El Niño events due to greenhouse warming *Nat. Clim. Change* **4** 111–6
Cai W *et al* 2021 Changing El Niño-Southern oscillation in a warming climate *Nat. Rev. Earth Environ.* **2** 628–44
Cai W *et al* 2022 Increased ENSO sea surface temperature variability under four IPCC emission scenarios *Nat. Clim. Change* **12** 228–31
Ceppi P, Hwang Y-T, Liu X, Frierson D M W and Hartmann D L 2013 The relationship between the ITCZ and the Southern Hemispheric eddy-driven jet *J. Geophys. Res.* **118** 5136–46
Collins M *et al* 2010 The impact of global warming on the tropical Pacific Ocean and El Niño *Nat. Geosci.* **3** 391–7
Denton G H, Anderson R F, Toggweiler J R, Edwards R L, Schaefer J M and Putnam A E 2010 The last glacial termination *Science* **328** 1652–6
Hoskins B J and Karoly D J 1981 The steady linear response of a spherical atmosphere to thermal and orographic forcing *J. Atmos. Sci.* **38** 1179–96
Huang P and Xie S P 2015 Mechanisms of change in ENSO-induced tropical Pacific rainfall variability in a warming climate *Nat. Geosci.* **8** 922–6
Hurrell J W *et al* 2013 The community earth system model: a framework for collaborative research *Bull. Am. Meteorol. Soc.* **94** 1339–60
Hyun S-H, Yeh S-W, Kirtman B P and An S-I 2022 Internal climate variability in the present climate and the change in ENSO amplitude in future climate simulations *Front. Clim.* **4** 932978
Kim S *et al* 2014 Response of El Niño sea surface temperature variability to greenhouse warming *Nat. Clim. Change* **4** 786–90
Kohyama T, Hartmann D L and Battisti D S 2017 La Niña-like mean-state response to global warming and potential oceanic roles *J. Clim.* **30** 4207–25
Kug J-S *et al* 2022 Hysteresis of the intertropical convergence zone to CO_2 forcing *Nat. Clim. Change* **12** 47–53
Kug J-S, An S-I, Ham Y-G and Kang I-S 2010 Changes in El Niño and La Niño teleconnections over North Pacific-America in the global warming simulations *Theor. Appl. Climatol.* **100** 275–82

Lawrence D M *et al* 2011 Parameterization improvements and functional and structural advances in version 4 of the community land model *J. Adv. Model. Earth Syst.* **3** M03001
Lindzen R S and Nigam S 1987 On the role of sea surface temperature gradients in forcing low-level winds and convergence in the tropics *J. Atmos. Sci.* **44** 2418–36
Liu C *et al* 2023a Hysteresis of the El Niño-Southern oscillation to CO_2 forcing *Sci. Adv.* **9** eadh8442
Liu C *et al* 2023b ENSO skewness hysteresis and associated changes in strong El Niño under a CO_2 removal scenario *npj Clim. Atmos. Sci.* **6** 117
Lou J, O'Kane T J and Hobrook N J 2021 Linking the atmospheric Pacific-South American mode with oceanic variability and predictability *Commun. Earth Environ.* **2** 223
Neale R B *et al* 2012 Description of the NCAR community atmosphere model (CAM 5.0) *NCAR Technical Note* TN-486 p 274
O'Kane T J, Monselesan D P and Risbey J S 2017 A multiscale reexamination of the Pacific-South American pattern *Mon. Weather Rev.* **145** 379–402
Olson R, Kim S-K, Fan Y and An S-I 2022 Probabilistic projections of El Niño Southern Oscillation properties accounting for model dependence and skill *Sci. Rep.* **12** 22128
Perry S J, McGregor S, Gupta A S and England M H 2017 Future changes to El Niño–Southern oscillation temperature and precipitation teleconnections *Geophys. Res. Lett.* **44** 10608–16
Power S B, Delage F, Chung C T, Kociuba G and Keay K 2014 Robust twenty-first century projections of El Niño and related precipitation variability *Nature* **502** 541–7
Shin N-Y *et al* 2022 More frequent central Pacific El Niño and stronger eastern pacific El Niño in a warmer climate *npj Clim. Atmos. Sci.* **5** 101
Simmons A J, Wallace J M and Branstator G W 1983 Barotropic wave propagation and instability, and atmospheric teleconnection patterns *J. Atmos. Sci.* **40** 1363–92
Smith R D *et al* 2010 The parallel ocean program (POP) reference manual: ocean component of the community climate system model (CCSM) and community earth system model (CESM) *Report LAUR*-10-01853 (Los Alamos National Laboratory Technical) p 141
Timmermann A *et al* 2018 El Niño–Southern oscillation complexity *Nature* **559** 535–45
Ting M and Yu L 1998 Steady Response to Tropical Heating in Wavy Linear and Nonlinear Baroclinic Models *J. Atmos. Sci.* **55** 3565–82
Wang Y *et al* 2022 Understanding the Eastward shift and intensification of the ENSO teleconnection over South Pacific and Antarctica under greenhouse warming *Front. Earth Sci.* **10** 916624
Wang Y, Hu K, Huang G and Tao W 2021 Asymmetric impacts of El Niño and La Niña on the Pacific-North American teleconnection pattern: the role of subtropical jet stream *Environ. Res. Lett.* **16** 114040
Watanabe M and Kimoto M 2000 Atmosphere-ocean thermal copuling in the North Atlantic: a positive feedback *Q. J. R. Meteorol. Soc.* **126** 3343–69
Yan Z, Wu B, Li T, Collins M, Clark R, Zhou T, Murphy J and Tan G 2020 Eastward shift and extension of ENSO-induced tropical precipitation anomalies under global warming *Sci. Adv.* **6** eaax4177
Yeh S-W *et al* 2018 ENSO atmospheric teleconnections and their response to greenhouse gas forcing *Rev. Geophys.* **56** 185–206
Yeh S-W, Kug J-S and An S-I 2014 Recent progress on two types of El Niño: observations, dynamics, and future changes *Asia Pac. J. Atmos. Sci.* **50** 69–81